IJME

Int. J. of Applied Mechanics and Engineering, 2025, vol.30, No.4, pp.104-124
DOI: 10.59441/ijame/209466

COMPARATIVE ANALYSIS OF EROSION-CORROSION IN STAINLESS STEELS: EVALUATING AISI 304, AISI 316, AND UB6 ACROSS VARIED CORROSIVE CONDITIONS

K. Mesbah*, B. Ouaki, M.K. El Kouifat and G. Ayad
Material Engineering Laboratory, The National Higher School of Mining of Rabat (ENSMR), MOROCCO
E-mail: mesbah.khaoula@gmail.com

This study investigates the erosion-corrosion behavior of stainless steels AISI 304, AISI 316, and UB6 (AISI 904L) under various impact angles and environmental conditions (neutral, saline, and acidic). The research focuses on assessing material resistance, analyzing the influence of impact parameters and environments on degradation, and exploring the synergy between erosion and corrosion. Results show that AISI 304 exhibits the highest degradation, particularly at a *45°* impact angle in acidic conditions. AISI 316 demonstrates moderate resistance, with greater sensitivity in saline and acidic media, while UB6 shows better resistance. Experiments were conducted using a custom test bench designed at the Materials Engineering Laboratory. Statistical analysis (ANOVA) of results showed the significant effects of impact angle and environment on mass loss of chosen material for test.

Key words: corrosive environment, corrosion, erosion-corrosion, impact angle, mass loss, stainless steel.

1. Introduction

Erosion-corrosion of stainless steels is a complex phenomenon that combines mechanical wear and chemical degradation, often observed in aggressive environments–such as marine, petrochemical, and water treatment settings–leading to accelerated material deterioration that compromises their lifespan and increases maintenance costs. Although stainless steels are widely used for their resistance to both corrosion and erosion, they can nonetheless be vulnerable to erosion-corrosion under certain specific operating conditions.

The phenomenon of erosion-corrosion is influenced by multiple factors, including particle impact velocity, impact angle, chemical composition of materials, and operating conditions. Previous research has identified key degradation mechanisms and parameters affecting the erosion-corrosion resistance of stainless steels. For instance, López *et al*. [1] demonstrated that for AISI 304 stainless steel, moderate degradation occurs at low impact velocity (*4.5 m/s*) under normal incidence, while severe degradation arises at higher velocities (*8.5 m/s*) and at oblique angles, with dominant plastic deformation mechanisms. Ghasemi *et al*. [2] and Rajahram *et al*. [3] further showed that the optimal angle for maximum erosion ranges between *25°* and *30°*, promoting increased plastic deformation, particularly in simulated marine environments.

In contrast, some studies have observed a strong synergy between erosion and corrosion at moderate impact angles, such as *60°* and *45°* [4-7]. Additionally, Chung *et al*. [8] demonstrated that for duplex stainless steels, perpendicular impact favors a homogeneous pressure distribution. At lower angles, such as *20°* and *45°*, erosion becomes more significant due to increased abrasion from particle sliding, thereby highlighting that the effect of impact angle can vary depending on the material and the surrounding environment.

The chemical composition and microstructure of stainless steels play a pivotal role in determining their resistance to erosion-corrosion. Iversen and Leffler [9] demonstrated that alloying elements such as chromium and molybdenum are essential for enhancing corrosion resistance. Chromium fosters the formation of a protective passive film, while molybdenum improves resistance to pitting and mechanical erosion [6, 10].

* To whom correspondence should be addressed

Additionally, the material's microstructure significantly influences the prevailing wear mechanisms, further shaping its overall durability under erosive and corrosive conditions [7, 11].

Furthermore, both hardness and surface roughness play key roles in the erosion and corrosion resistance of stainless steels. Ricardo and Sommerfeld [12] observed that surface roughness increases with the angle of inclination and erosion time. Divakar *et al*. [13] demonstrated that enhancing the hardness of AISI 316 stainless steel significantly improves its erosion resistance by delaying crater formation and reducing mass loss–a relationship further confirmed by Malik *et al*. [14]. However, Malik *et al*. [14] noted that this relationship is not strictly linear due to the influence of microstructure.

Regarding surface roughness, Bassach *et al*. [15] found that rougher surfaces degrade more rapidly in saline environments, as they provide more sites for corrosion initiation. On the other hand, Toloei *et al*. [16] showed that extremely smooth surfaces can sometimes encourage the formation of non-protective passive films, underscoring the complexity of roughness effects on corrosion resistance.

In addition, the nature of the corrosive environment significantly influences the erosion-corrosion resistance of stainless steels. Loto [17] compared the performance of 304L and 316 stainless steels in hydrochloric acid solutions with varying chloride concentrations. Their study demonstrated that AISI 316, due to its molybdenum content, exhibits greater resistance in chloride-rich environments, while AISI 304L is more susceptible to pitting and rapid degradation. Similarly, Zhang *et al*. [18] confirmed that chloride-containing environments accelerate localized corrosion, with the presence of chlorides promoting pitting corrosion [19-21] However, in environments containing sulfate, partial stabilization of the passive film can sometimes reduce the overall corrosion rate, highlighting the complex interplay of ions in the corrosive medium.

In high-temperature acidic solutions, Lindgren *et al*. [22] observed that 904L stainless steel (UB6) outperforms other austenitic steels, such as 316L, due to its ability to rapidly passivate. Yao *et al.* [10] specifically examined the effects of chloride ions on the erosion-corrosion behavior of 316L stainless steel in a flow jet impingement setup. Their findings were corroborated by Li *et al*. [23], who modeled the behavior of AISI 316 under high-temperature, high-velocity particle impacts, showing how such conditions can significantly alter corrosion resistance.

The synergistic effect between erosion and corrosion remains a critical yet poorly understood factor. Neshati and Shirazani [24] reported high synergy at moderate impact angles, while Andrews *et al*. [25] observed a peak synergy at lower angles (*30°* to *45°*) for SS316 stainless steel in a NaCl solution. This suggests that the impact angle plays a significant role in influencing the interaction between erosion and corrosion [15]. Furthermore, Zhao *et al*. [26] demonstrated that the presence of suspended solid particles, such as marine sand in a saline solution, significantly increases the erosion-corrosion rate of 316 stainless steel, particularly at low impact angles. Chloride ions accelerate the breakdown of the protective passive film, promoting localized corrosion and weakening the surface, which makes it more susceptible to mechanical damage.

The synergy between erosion and corrosion arises from interdependent mechanisms, where mechanical erosion removes protective passive films or oxide layers, thereby exposing metal surfaces to accelerated chemical attack, while corrosion simultaneously weakens the material's surface, increasing its vulnerability to mechanical damage [27]. This interplay is particularly severe in environments containing aggressive ions such as Cl^- and H^+, where localized corrosion (e.g., pitting) exacerbates surface roughening and enhances erosion rates [28]. The synergy factor, defined as the difference between the total erosion-corrosion mass loss and the sum of the individual losses from pure erosion and pure corrosion, quantifies this interaction. Importantly, this relationship is not merely additive; rather, the coupling of erosion and corrosion leads to a synergistic effect that significantly accelerates material degradation. Understanding and accurately quantifying this synergy is essential for optimizing alloy performance in aggressive industrial environments.

In addition, Brownlie *et al*. [29] showed that damage in the direct impact zone (DIZ) is primarily caused by mechanical erosion, while the peripheral outer area (OA) experiences a greater influence from the combined interactions of erosion and corrosion. This highlights the spatial variability in the mechanisms driving erosion-corrosion, depending on the region of the material exposed to the jet.

These observations highlight the complexity of the combined effects of mechanical parameters and corrosive environments on material behavior under erosion-corrosion.

Despite advancements in understanding the factors influencing erosion-corrosion, several aspects remain underexplored, particularly the complex interactions between erosion and corrosion. Further analysis of these interactions could provide valuable insights into the resistance of stainless steels to erosion-corrosion in various environments.

This study aims to assess the resistance of AISI 304, AISI 316 L, and UB6 (AISI 904L) stainless steels to erosion-corrosion and to investigate the underlying microstructural degradation mechanisms. AISI 904L, in particular, has received less attention in the literature despite its potential advantages in aggressive environments, making it a focal point of this work.

Controlled experimental tests were performed to evaluate the influence of impact angle and environmental conditions (neutral, saline, and acidic) on the degradation of these steels. The study examines the synergy between erosion and corrosion by quantifying key metrics such as mass loss, surface roughness, and material hardness under various operating conditions. This research seeks to provide a deeper understanding of the factors driving the erosion-corrosion behavior of these materials, while addressing the knowledge gap regarding the performance of AISI 904L in highly corrosive conditions.

2. Materials and methods

2.1. Material

This study examines the performance of three stainless steels: AISI 304, AISI 316L, and UB6 (AISI 904L), selected for their erosion-corrosion resistance properties. The table below summarizes the chemical composition of each alloy in mass percentage:

Table 1. Compositions of the AISI 304, AISI 316L and UB6 stainless steels used (wt.%).

Grade	C *(%)*	Cr *(%)*	*Ni (%)*	Mo *(%)*	Mn *(%)*	Si *(%)*	P *(%)*	S *(%)*	Cu *(%)*
AISI 316L	*0.02*	*16.87*	*12.73*	*2.69*	*1.51*	*0.60*	*0.030*	*0.005*	*0.18*
AISI 304	*0.08*	*18.14*	*8.35*	*0.23*	*1.74*	*0.55*	*0.035*	*0.005*	*0.23*
UB6 / AISI 904L	*0.019*	*20.3*	*24.7*	*4.4*	*1.60*	*0.35*	*0.022*	*0.001*	*1.50*

The abrasive particles used to simulate erosion have an average size of *0.23 mm* and consist of *99.7%* silica (Fig.1).

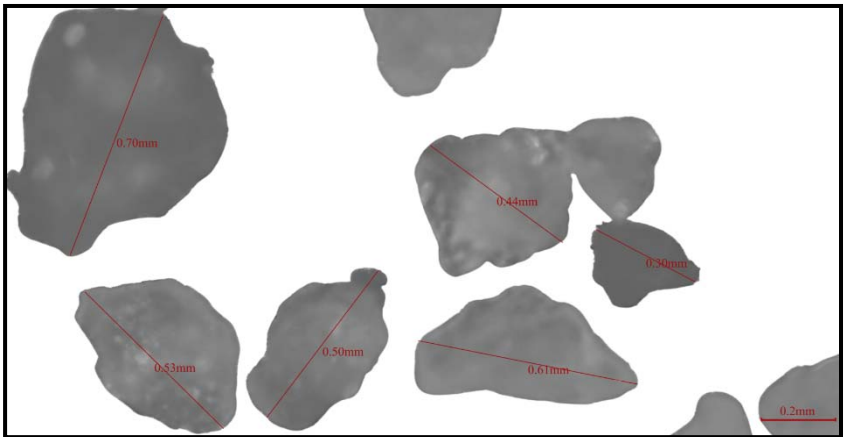

Fig.1. SEM image of particle sizes.

2.2. Sample preparation

The samples, measuring *25 mm* × *45 mm* × *5 mm*, were polished using silicon carbide (SiC) abrasive papers with successive grit sizes ranging from *80* to *1000*. The polishing was performed in the same direction for all samples. After polishing, the samples were rinsed with diluted water, air-dried and stored in protective sleeves to prevent oxidation before testing.

To ensure accurate mass loss measurements during testing, PTFE (Teflon) tape was carefully applied around the edges of each specimen to seal the non-exposed surfaces, leaving only one face unsealed and exposed to the test medium. Subsequently, the specimens were partially embedded in epoxy resin on the PTFE tape, ensuring that only the exposed surface remained in contact with the abrasive jet. Since neither the resin nor the tape was subjected to direct jet impact, their presence did not interfere with the erosion process and allowed for easy removal after testing without altering the analyzed surface.

Following the erosion-corrosion tests, the samples were sectioned perpendicularly to the exposed face for microstructural examination. A standard metallographic mounting procedure was applied to the cross-sections, ensuring that the internal structure in the erosion zone was visible. Electrochemical etching was then performed using a *10%* oxalic acid solution in distilled water, applying a voltage of *6 V* for *20* seconds. Etching was confined to the cross-sectional surface and carried out using a cotton swab to maintain localized control and effectively reveal grain boundaries.

2.3. Test conditions for simple erosion and erosion-corrosion

Erosion test:

The erosion tests were conducted in a:

Neutral medium: Diluted water with *2%* silica particles, *pH 7.2*, at a temperature of *25.4°C*. The AISI 304 samples were first exposed to abrasive jets at three impact angles (*30°*, *45°*, and *60°*), with the test duration set to *5* hours. Mass loss and surface roughness were measured at regular intervals (every *1* hour) to monitor sample degradation and identify the most critical angle.

A second test was then conducted at the selected angle (**45°**) on **AISI 304, AISI 316L, and UB6**, under the same conditions, to compare their erosion resistance.

Erosion-corrosion test:

The erosion-corrosion tests were conducted in three different media to simulate severe industrial environments:

- *Neutral medium*: Distilled water with *2%* silica particles with *pH=7.27*, at a temperature of *25.3°C*.
- *Saline medium*: Distilled water with *3%* NaCl and *2%* abrasive particles with *pH=6.96*, at a temperature of *26.7°C*.
- *Acidic medium*: Distilled water with *13%* phosphoric acid, *7%* sulfuric acid and *2%* abrasive particles with *pH 0.11*, at a temperature of *44.7 °C*.

A series of measurements were conducted at regular intervals to monitor sample degradation. Each test included sequential steps, starting with the measurement of open circuit potential (OCP) followed by linear voltammetry to assess the electrochemical activity of the samples. Subsequently, the samples were subjected to an abrasive jet at a *45°* angle for one hour without interruption or removal from the medium, ensuring a continuous transition between the corrosion and erosion.

The electrochemical testing procedure was conducted in a sequential manner, as illustrated in Fig.3 and included the following steps:

a. **Set up the Three-Electrode Electrochemical Cell:**
   - *Working Electrode* (*WE*): The stainless steel sample (AISI 304, AISI 316L, UB6) exposed to erosion-corrosion.
   - *Reference Electrode (SCE, Saturated Calomel Electrode):* Ensures a stable potential to monitor changes in the working electrode.
   - *Auxiliary Electrode (Platinum):* Completes the circuit, enabling current flow without influencing the working electrode.

b. **Corrosion test**: Measuring the open circuit potential (OCP) and conducting linear sweep voltammetry to evaluate electrochemical activity.

c. Electrochemical Test Parameters:

The Open Circuit Potential (OCP) measurements were carried out for a duration of *4* minutes, with a data acquisition interval of *0.2* seconds. The system was configured to record all points without applying any polarization at the end of the test.

Linear sweep voltammetry (LSV) was then performed over a potential range from $-3000\ mV$ to $+3000\ mV$ (to fully capture the anodic and cathodic branches of the polarization curve for all three steels.) vs. REF, using a scan rate of *1.8 mV/s*, with intermediate steps set at *200 mV/s* and *0.009 mV/s* for precision. The current range was set between $-2000\ mA$ and $+2000\ mA$.

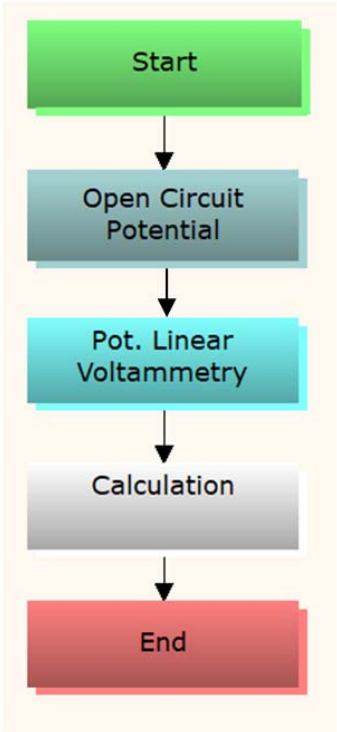

Fig.2. Electrochemical testing sequence.

d. **Abrasive Jet Exposure:** Applying an abrasive jet at a *45°* angle for one hour without interruption.

e. **Post-Jet Corrosion Test:** Repeating the corrosion testing sequence to assess any changes.

Physical degradation was quantified by measuring mass loss and surface roughness before and after exposure to the abrasive jet. Each test was repeated three times to ensure accuracy, with the average values used to compare surface degradation and the relative resistance of the steels under severe erosion-corrosion conditions.

2.4. Equipment and measurements

The instrumentation used for the experiment includes:

- *OrigaMaster 5 potentiostat* (Fig.3): Used for electrochemical measurements, such as open circuit potential (OCP) and linear voltammetry, to evaluate the corrosion activity of the samples in each medium.
- *Precision balance* (accuracy of *0.01 mg*): Used to measure the mass loss of the samples before and after the tests.

- *Surface roughness meter*: Employed to measure the surface roughness of the samples after each test, providing information on surface erosion.
- *pH meter*: Used to verify and adjust the pH of the test solutions before each experiment to ensure consistent conditions.
- *Optical microscope*: Enables continuous observation of the microstructure of samples before and after each test, facilitating visual exam of surface changes after test.

2.5. Test bench

The test bench is custom-designed and was built in the Materials Engineering laboratory at the École Nationale Supérieure des Mines de Rabat to simulate the phenomenon of erosion-corrosion (Fig.3). It includes:

- a solution tank with a circulation pump,
- an adjustable sample holder that allows impact angle adjustments,
- a protractor for impact angle adjustments,
- a support for the electrodes,
- solution circuit tubing,
- jet nozzle: directs the water jet mixed with abrasive particles straight onto the sample.

(With nozzel size = *10 mm* and velocity = *1 m/s*).

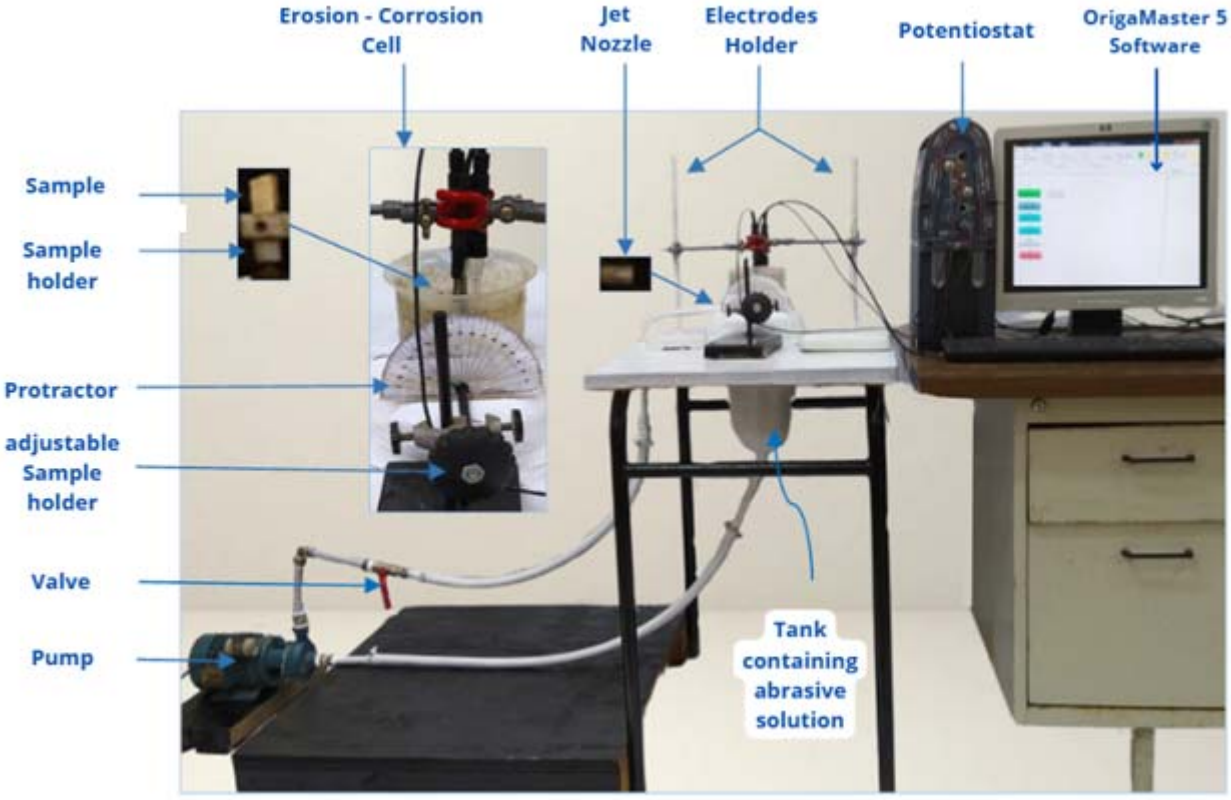

Fig.3. Erosion test bench.

2.6. Statistical analysis

The ANOVA analysis was conducted using the 'Two-Factor ANOVA with Replication' function in the Excel Analysis ToolPak (Microsoft Excel, version 2016), which provides a straightforward approach for

conducting ANOVA on data with repeated measures. The obtained mass loss data were analyzed to evaluate the statistically significant impact of various experimental variables, such as impact angle and corrosive environment. This analysis helped identify the factors with the most influence on material degradation rates.

3. Results

This section presents the results of three tests conducted to evaluate the resistance of stainless steels AISI 304, AISI 316, and UB6 under various erosion and erosion-corrosion conditions. Each test focuses on a specific aspect of these alloys' resistance, including pure erosion and combined erosion-corrosion behavior.

3.1. Results of pure erosion test: AISI 304 under different impact angles in a neutral environment

The first test was designed to examine the influence of impact angle on the erosion behavior of stainless steel AISI 304 in a neutral environment (diluted water) over a *5*-hour period. Three impact angles (*30°*, *45°* and *60°*) were tested to assess how varying the angle affects the material's degradation. Mass loss and surface roughness measurements were taken every hour to track the progression of erosion.

- *Mass loss ratio* $(\Delta m / m_o)$: This ratio represents the relative mass loss (Δm) compared to the initial mass m_o of the sample. Here, Δm refers to the mass lost by the sample due to erosion, and the ratio $\Delta m / m_o$ provides an indication of the severity of degradation. Higher values of $\Delta m / m_o$ indicate more significant erosion.
- *Roughness ratio* $(\Delta R / R_o)$: This ratio represents the change in surface roughness of the sample after exposure to erosion conditions. ΔR is the change in roughness from the initial roughness (R_o) measured before testing. The ratio $\Delta R / R_o$ offers insights into the surface morphology evolution, where an increase in $\Delta R / R_o$ signifies a rougher surface due to erosion.

Table 2. Mass loss and ratio and roughness ratio of AISI 304 stainless steel in a neutral medium at various impact angles.

Time (*h*)	AISI 304 / *30°*		AISI 304 / *45°*		AISI 304 / *60°*	
	mass loss ratio 10^{-5} $(\Delta m / m_o)$	roughness ratio $(\Delta R / R_o)$	mass loss ratio 10^{-5} $(\Delta m / m_o)$	roughness ratio $(\Delta R / R_o)$	mass loss ratio 10^{-5} $(\Delta m / m_o)$	roughness ratio $(\Delta R / R_o)$
1	*2.01*	*0.31*	*3.19*	*0.34*	*1*	*0.18*
2	*3.32*	*0.42*	*5.47*	*0.48*	*1.66*	*0.2*
3	*5.32*	*0.44*	*7.02*	*0.64*	*2.34*	*0.25*
4	*5.9*	*0.46*	*7.84*	*0.66*	*2.61*	*0.3*
5	*6.31*	*0.54*	*7.94*	*0.75*	*2.65*	*0.30*

The results show that the *45°* impact angle results in the highest mass loss, followed by the *30°* angle, while the *60°* angle produces the lowest mass loss (Fig.4). This suggests that the *45°* angle promotes more intense erosion, likely due to an optimal combination of tangential and impact forces.

Surface roughness was also measured to assess the effect of impact angle on the condition of the surface after erosion (Fig.5). The results indicate that the *45°* angle leads to a more pronounced increase in roughness, confirming that this impact angle causes greater surface degradation of the AISI 304 steel.

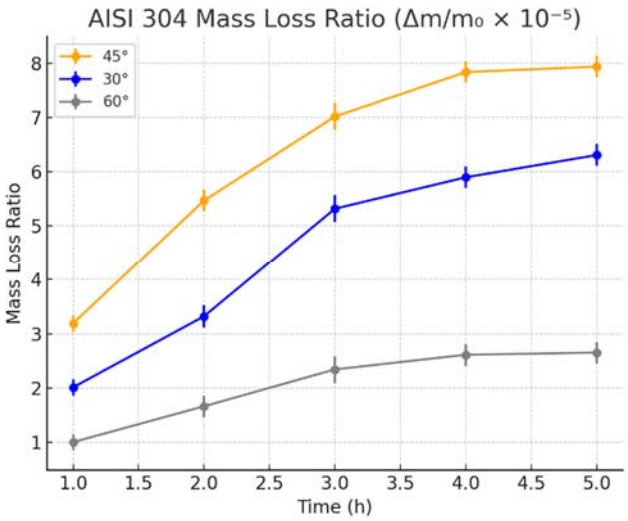

Fig.4. Evolution of AISI 304 mass loss ratio $10^{-5}\ (\Delta m / m_o)$.

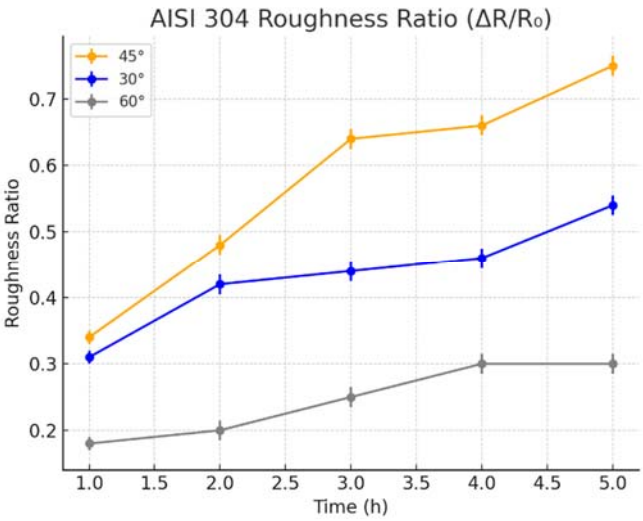

Fig.5. Evolution of AISI 304 roughness ratio $(\Delta R / R_o)$.

3.2. Results of simple erosion test: comparison of AISI 304, AISI 316, and UB6 stainless steels in a neutral medium at a *45°* impact angle

The results of this second test allow for a comparison of the erosion resistance of stainless steels AISI 304, AISI 316 and UB6 in a neutral medium at a *45°* impact angle over a period of *5* hours (Tab.3).

Table.3. The mass ratio $(\Delta m / m_o)$ and the roughness ratio $(\Delta R / R_o)$ for AISI 304, AISI 316, and UB6 steels in a neutral medium at a *45°* impact angle.

Time (*h*)	AISI 304 / *45°*		AISI 316L / *45°*		UB6 / *45°*	
	mass loss ratio 10^{-5} $(\Delta m / m_o)$	roughness ratio $(\Delta R / R_o)$	mass loss ratio 10^{-5} $(\Delta m / m_o)$	roughness ratio $(\Delta R / R_o)$	mass loss ratio 10^{-5} $(\Delta m / m_o)$	roughness ratio $(\Delta R / R_o)$
1	*3.19*	*0.29*	*1.92*	*0.14*	*1*	*0.08*
2	*4.47*	*0.48*	*2.68*	*0.23*	*1.39*	*0.13*
3	*7.02*	*0.56*	*4.21*	*0.28*	*2.25*	*0.16*
4	*7.84*	*0.6*	*4.71*	*0.28*	*2.51*	*0.17*
5	*7.94*	*0.62*	*4.76*	*0.31*	*2.52*	*0.2*

At a *45°* impact angle, AISI 304 exhibits the highest mass loss, followed by AISI 316, while UB6 demonstrates the lowest mass loss over the *5*-hour testing period (Fig.6). This trend indicates that UB6 has the highest resistance to erosion in a neutral medium under these conditions, whereas AISI 304 is the most susceptible to corrosion process. These findings highlight that UB6 is better suited for erosion conditions, confirming that alloys with a high percentage of chromium and molybdenum offer better resistance to erosion.

Additionally, the roughness ratio follows a similar pattern, with AISI 304 showing the greatest increase in surface roughness, AISI 316L displaying moderate roughness evolution, and UB6 experiencing the smallest degradation (Fig.7). This demonstrates that UB6 not only has the lowest mass loss but also exhibits the best resistance to surface degradation, while AISI 304 undergoes the most significant surface roughening.

Overall, these results confirm that UB6 had the most resistant to erosion in a neutral medium, followed by AISI 316L, with AISI 304 being the least resistant to erosion-corrosion.

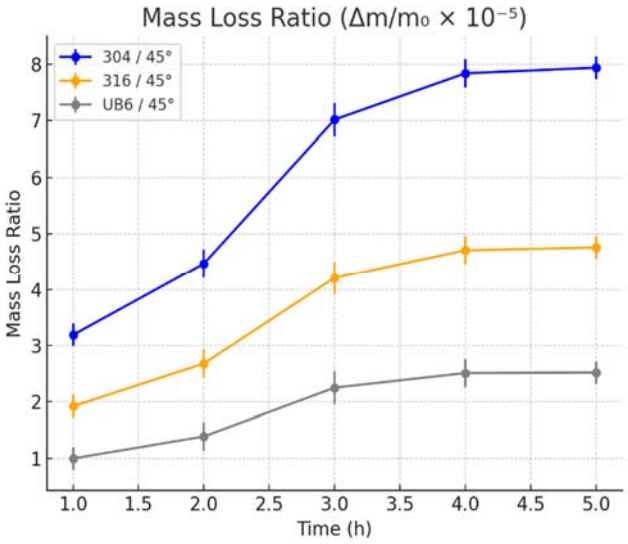

Fig.6. Evolution of AISI 304, AISI 316L and UB6 mass loss ratio 10^{-5} $(\Delta m / m_o)$ under a $45°$ impact angle in a neutral medium.

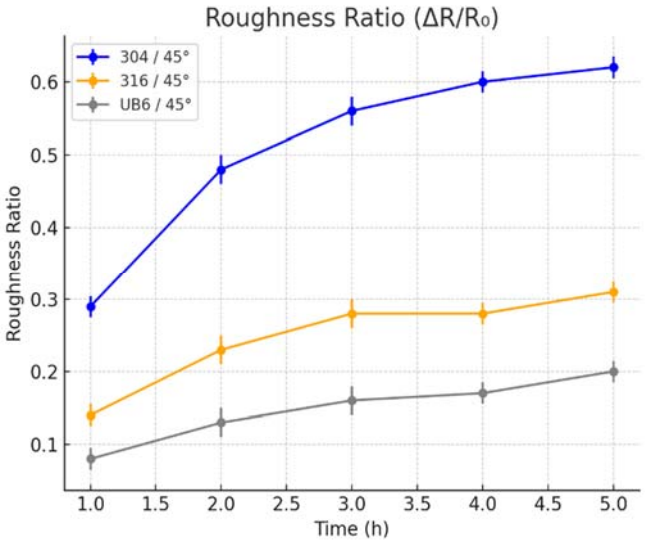

Fig.7. Evolution of AISI 304 roughness ratio $(\Delta R / R_o)$ under a 45° impact angle in a neutral medium.

Hardness

After the erosion tests, surface hardness measurements were conducted to evaluate the effect of abrasive impacts on the samples. The evolution of surface hardness for AISI 304, AISI 316L, and UB6 exposed to erosion in a neutral medium was analyzed to assess their hardening under abrasion. Vickers hardness was measured three times at the end of erosion tests conducted in distilled water (DIW) at a $45°$ angle, and the average values were determined. The results were reported in Tab.6 bellow.

Table 6. Hardness measurements after the erosion test.

	AISI 304	AISI 316L	UB6 (AISI 904L)
Hardness (*HV*) (before test $t = 0$)	*149*	*152*	*160*
Hardness (*HV*) (after test $t = 5h$)	*182.85*	*169.88*	*165.37*

The results show that AISI 304 exhibits the most significant increase in hardness after the erosion tests, followed by AISI 316 and then UB6. This is likely due to work hardening caused by abrasive impacts. The slightly higher hardness of AISI 304 can be attributed to its greater susceptibility to surface deformation and roughening under abrasion. In contrast, UB6, which shows the lowest level of hardening, demonstrates its better resistance to erosion-corrosion in neutral environments.

3.3. Erosion-corrosion test results: AISI 304, AISI 316L and UB6 in neutral, saline and acidic environments at a *45°* angle.

The third test combines erosion and corrosion by subjecting the samples to an abrasive particle jet for one hour at a *45°* impact angle in three different corrosive environments: neutral, saline (NaCl) and acidic. After the test, mass loss and surface roughness were measured to assess the material degradation due to the combined effects of erosion and corrosion.

The results (Fig.8 and Fig.9) show that mass loss is highest in the acidic environment, followed by the saline environment, and lowest in the neutral environment for all materials. AISI 304 is the most affected in all environments, confirming its vulnerability to acid attacks, while UB6 shows the lowest mass loss, demonstrating its better resistance to erosion-corrosion in environment tests.

Table 4. Mass loss ratio $(\Delta m / m_o)$ and roughness ratio $(\Delta R / R_o)$ after the abrasion test in the three environments (neutral, saline, acidic)

	AISI 304 / *45°*		AISI 316L / *45°*		UB6 / *45°*	
	mass loss ratio 10^{-5} $(\Delta m / m_o)$	roughness ratio $(\Delta R / R_o)$	mass loss ratio 10^{-5} $(\Delta m / m_o)$	roughness ratio $(\Delta R / R_o)$	mass loss ratio 10^{-5} $(\Delta m / m_o)$	roughness ratio $(\Delta R / R_o)$
neutral environment	*3.20*	*0.3*	*2.05*	*0.14*	*1.57*	*0.085*
saline environment	*4.77*	*0.43*	*3.86*	*0.3*	*3*	*0.11*
acidic environment	*6.04*	*0.61*	*5.014*	*0.36*	*4.17*	*0.18*

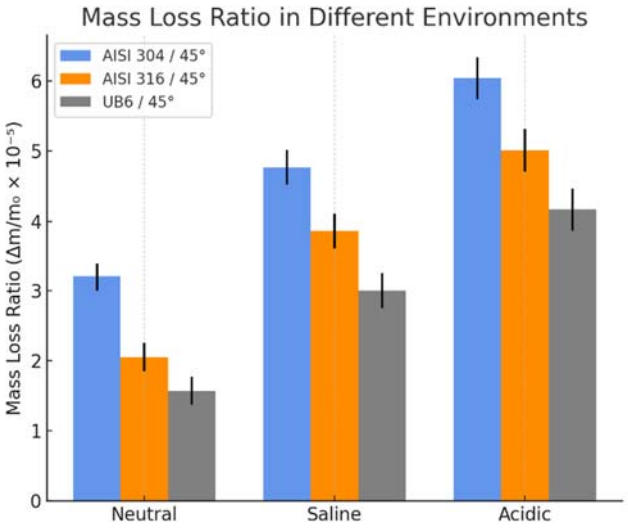

Fig.8. Evolution of AISI 304, 316 and UB6 mass loss ratio 10^{-5} $(\Delta m / m_o)$ under a *45°* impact angle in the three environments (neutral, saline, acidic).

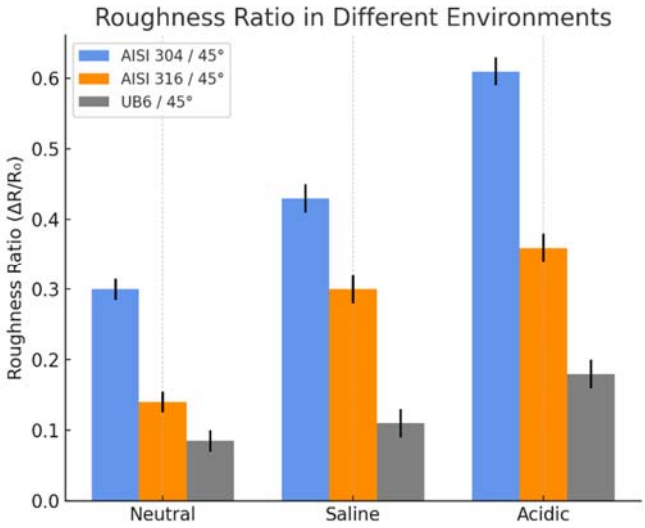

Fig.9. Evolution of AISI 304 roughness ratio $(\Delta R / R_o)$ under a *45°* impact angle in the three environments (neutral, saline, acidic).

Similarly, the roughness results reveal that AISI 304 is the most susceptible to erosion-corrosion regardless of the environment, with the roughness ratio reaching its maximum in the acidic medium. In contrast, UB6 offers the best resistance, showing minimal surface roughening in all tested environments.

These findings highlight the synergy between erosion and corrosion, especially in the acidic environment, and establish a clear hierarchy of performance among the tested materials: AISI 304 is the most vulnerable, followed by AISI 316L, while UB6 demonstrates the best overall resistance to erosion-corrosion.

Open circuit potential (OCP)

The study of open circuit potential (OCP) is an indicator of the electrochemical stability of stainless steel alloys exposed to aggressive environments, both before and after abrasion. In this study, AISI 304, AISI 316L and UB6 stainless steels were subjected to OCP tests before and after exposure to an abrasive jet at a *45°* impact angle, in three different environments: neutral (distilled water), saline (NaCl) and acidic. The potential evolution curves (Figs. 10, 11 and 12) provide insight into the stability of the passive film and the ability of each material to resist electrochemical degradation.

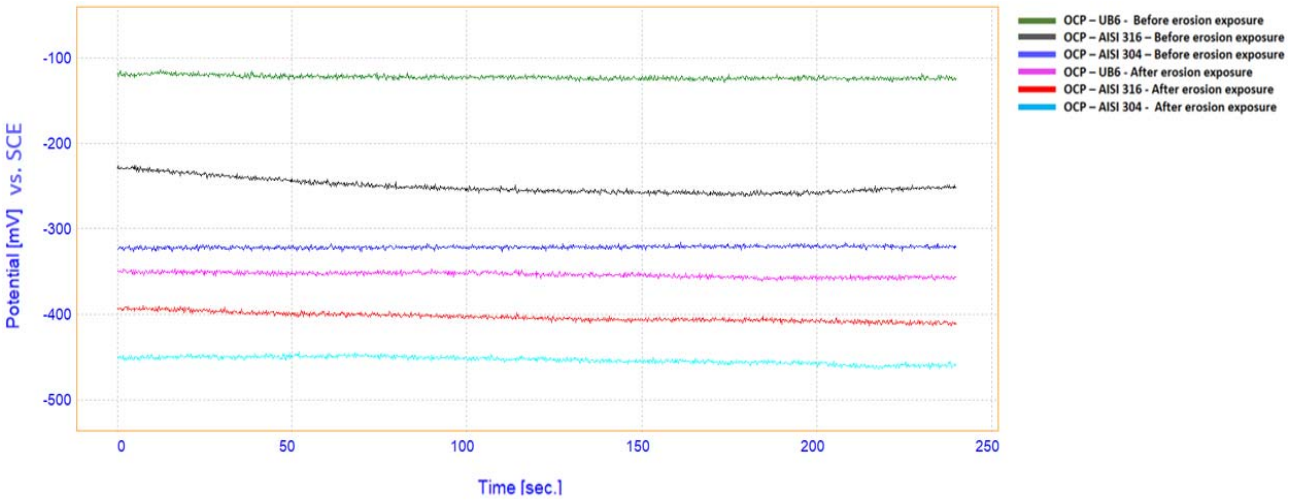

Fig.10. Open circuit potential (OCP) – neutral environment.

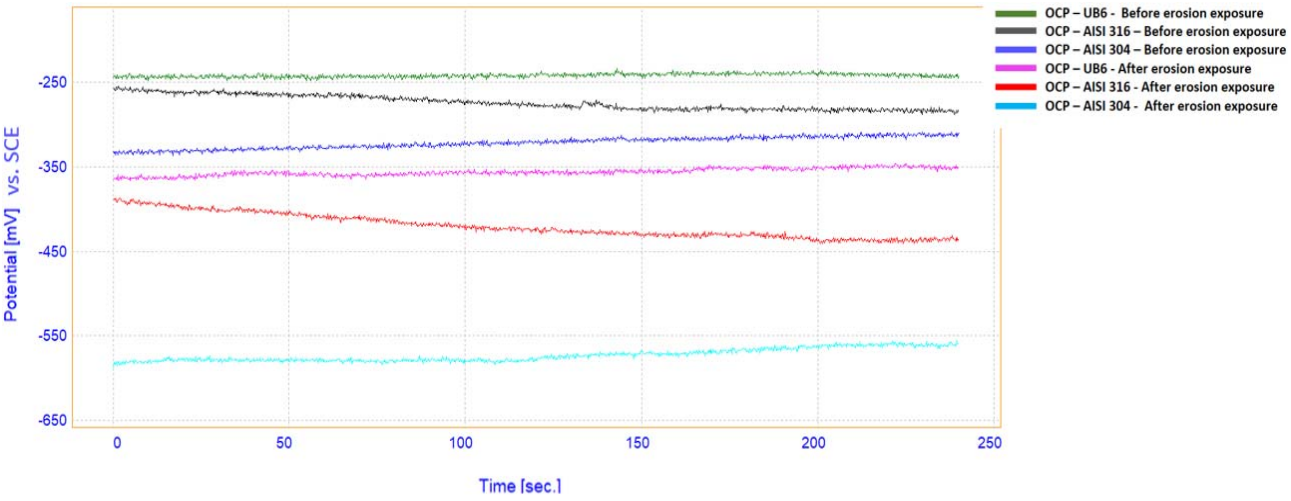

Fig.11. Open circuit potential (OCP) – NaCl environment.

Neutral environment (Fig.10): Before abrasion, all three stainless steels exhibit relatively stable potentials. The UB6 material shows a potential close to *–100 mV* vs. SCE, indicating the presence of a dense and protective passive film. AISI 316L stabilizes around *–200 mV*, while AISI 304 displays a more negative potential, around *–300 mV*, suggesting a more vulnerable passive state. After exposure to erosion, all materials experience a drop in potential. AISI 304 falls to approximately *–470 mV*, reflecting a significant breakdown of the passive layer. AISI 316L also shifts to around *–400 mV*, indicating degradation, though less severe than that of AISI 304. UB6 remains the most stable, with a potential around *–150 mV*, confirming its superior resistance to mechanical attack.

Saline environment (NaCl) (Fig.11): In the chloride-rich saline environment, corrosion is notably intensified. Before erosion, UB6 exhibits a relatively stable potential near *–250 mV*, while AISI 316L stabilizes around *–300 mV*. AISI 304 shows the most negative potential, approximately *–400 mV*, indicating a higher susceptibility to chloride-induced degradation. After erosion, AISI 304 experiences a pronounced drop to around *–600 mV*, reflecting a severe breakdown of the passive film. AISI 316L also shows a potential shift to about *–450 mV*, suggesting moderate degradation. In contrast, UB6 maintains a more stable potential near *–300 mV*, demonstrating superior electrochemical stability despite the aggressive saline conditions.

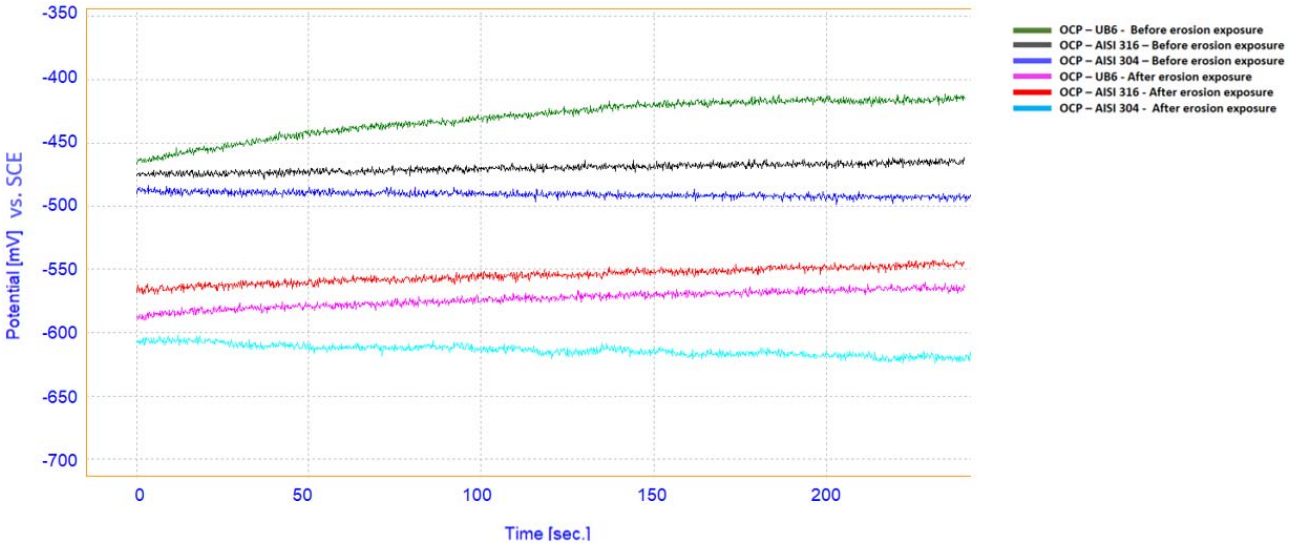

Fig.12. Open circuit potential (OCP) – acidic environment.

Acidic environment (Fig.12): The acidic environment proves to be the most aggressive toward passive films among the three media. Prior to abrasion, UB6 once again shows the highest stability, with a potential around *–440 mV*. AISI 316L and AISI 304 exhibit more negative values, at approximately *–470 mV* and *–500 mV* respectively. After abrasion, AISI 304 drops sharply to around *–650 mV*, indicating an almost complete loss of passive protection. AISI 316L also shows considerable degradation, reaching a potential of about *–550 mV*. UB6, although affected, retains a comparatively better electrochemical performance with a potential near *–500 mV*, underscoring its superior resistance even under highly aggressive acidic conditions.

Corrosion current density J_{corr}

To further analyze the synergistic effects of erosion and corrosion, the corrosion current density J_{corr} of the alloys was measured before and after exposure to the abrasive jet. As detailed in Tab.5, these values were extracted from polarization curves using linear sweep voltammetry and calculated via Tafel extrapolation. This parameter offers critical insights into the corrosion rates under varying environmental conditions, highlighting how the interplay between erosion and corrosion accelerates material degradation.

Results before abrasion (Fig.13.a): Prior to the abrasive jet test, AISI 304 exhibited the highest J_{corr} values across all environments, confirming its susceptibility to corrosion. AISI 316L showed moderate resistance with lower J_{corr} values than AISI 304 but higher than UB6. UB6 consistently displayed the lowest J_{corr} values, underscoring its better corrosion resistance and effective protective properties compared to the other alloys.

Table 5. Corrosion current density $J_{corr}\left(\mu A/cm^2\right)$ before / after exposure to an abrasive jet in the three environments (neutral, saline, acidic).

Environment	J_{corr} $\left(\mu A/cm^2\right)$ before (304)	J_{corr} $\left(\mu A/cm^2\right)$ after (304)	J_{corr} $\left(\mu A/cm^2\right)$ before (316)	J_{corr} $\left(\mu A/cm^2\right)$ after (316)	J_{corr} $\left(\mu A/cm^2\right)$ before (UB6)	J_{corr} $\left(\mu A/cm^2\right)$ after (UB6)
neutral environment	*15.27*	*25.59*	*13.99*	*16.58*	*10.83*	*12.32*
saline environment	*62.26*	*77.80*	*48.86*	*63.49*	*32.60*	*48.60*
acidic environment	*81.20*	*94.59*	*60.20*	*76.62*	*45*	*64.79*

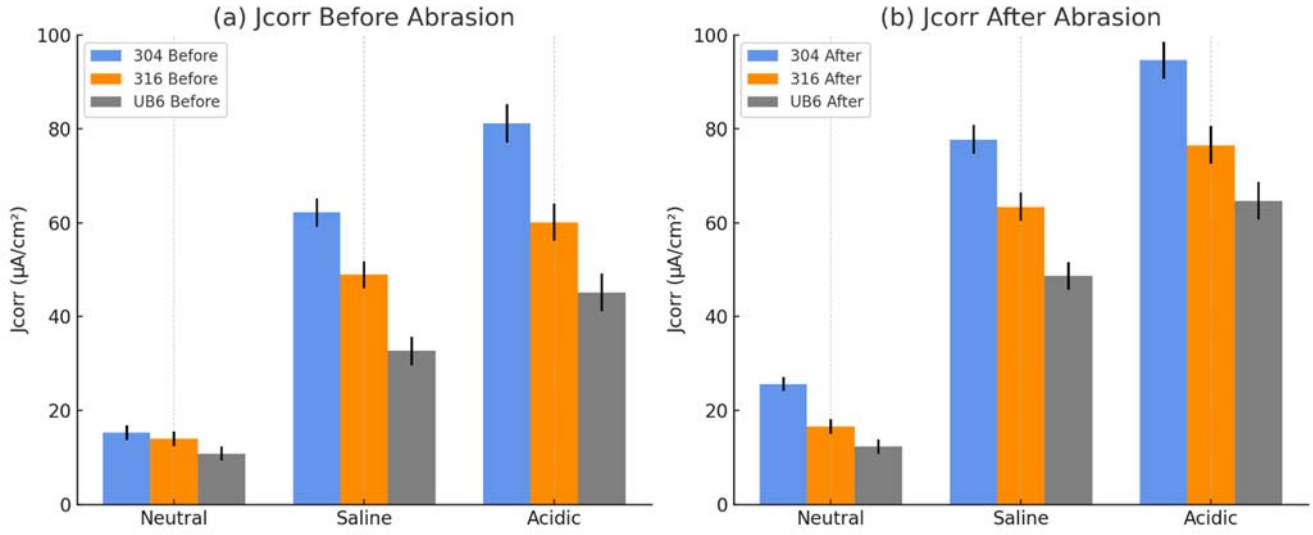

Fig.13. Corrosion current density $J_{corr}\left(\mu A/cm^2\right)$ before (a) and after (b) abrasion attack in the three environments (neutral, saline, acidic).

Results after abrasion (Fig. 13.b): After exposure to the abrasive jet, all alloys experienced a significant rise in J_{corr}, highlighting the synergistic effect of erosion and corrosion. This increase reflects the classic synergy mechanism, where erosion disrupts the passive film and corrosion attacks the newly exposed metal. The abrasive action likely damaged the protective surface layers, increasing the alloys' susceptibility to corrosion:

- Neutral environment: The increase in J_{corr} was relatively moderate. AISI 304 showed the highest increase, followed by AISI 316L, while UB6 remained the barely affected, maintaining the lowest J_{corr} values.

- Saline environment: A more pronounced increase in J_{corr} was observed, particularly for AISI 304, where chloride ions accelerated corrosion. AISI 316L and UB6 also experienced increased J_{corr}, but UB6 demonstrated the better resistance to corrosion in this environment.
- Acidic environment: The synergy between erosion and corrosion was most evident, with all alloys displaying their highest J_{corr} values. AISI 304 was again the most affected, followed by AISI 316L. Although UB6 showed an increase in J_{corr} under acidic conditions, it retained significantly lower values compared to the other alloys, demonstrating its better resistance.

Comparative performance of alloys

Overall, the combined analysis of mass loss, surface roughness, OCP, and J_{corr} highlights a clear performance hierarchy among the tested alloys. UB6 consistently demonstrated the best resistance to erosion-corrosion across all environments, with minimal mass loss, low roughness increase, stable electrochemical behavior, and the lowest J_{corr} values. AISI 316L showed intermediate performance, performing relatively well in neutral and saline environments but losing efficiency in acidic conditions. AISI 304 emerged as the most vulnerable alloy, with the highest degradation metrics in every tested scenario.

3.4 Results of the two-factor with replication statistical analysis (ANOVA)

F statistic is the ratio between the mean square of the factor (or interaction) and the mean square within the group. A high *F* value indicates that the factor has a significant effect on the response variable.
p-value (probability) indicates the likelihood that the observed effect occurred due to random variation. It is calculated based on the F statistic. If the *P* value is lower than (*0.05*), this indicates that the effect of the factor is statistically significant.
Critical F value is the reference point that the *F* statistic must exceed for the factor's effect to be considered statistically significant at the chosen significance level (*0.05*). If the F value exceeds the critical *F* value, it indicates that the factor has a significant effect.

Analysis 1: effect of impact angle and time on mass loss of AISI 304

This analysis evaluates the effect of impact angle (*30°*, *45°*, *60°*) and exposure time on the mass loss of AISI 304 stainless steel under simple erosion conditions. The results (Tab.6) confirm that both factors significantly influence mass loss, as shown by the ANOVA *p*-values.

Table 6. ANOVA analysis of the effects of impact angle on the mass loss of AISI 304 stainless steel.

Factor	*F*	Critical *F* value	*p*-value	Conclusion
Impact angle	*65.27*	*3.31*	$\ll 0.05$	The *45°* angle results in the highest mass loss for AISI 304, indicating maximum erosion at this angle.
Exposure time	*18.82*	*2.69*	$\ll 0.05$	Mass loss increases significantly with exposure time.
Interaction (angle × time)	*68.18*	*2.26*	$\ll 0.05$	The effect of impact angle is amplified over time, leading to accelerated degradation at a *45°* angle.

The impact angle has a strong effect, with an *F* value of *65.27* exceeding the critical value of *3.31*. The *45°* angle causes the highest mass loss, making it the most critical for erosion. Exposure time also significantly

affects mass loss, with an F value of *18.82* exceeding the critical value of *2.69*, showing that degradation increases consistently over time.

The interaction between impact angle and exposure time, with an F value of *68.18* exceeding the critical value of *2.26*, indicates that the effect of angle is amplified over time, particularly at *45°*, where combined effects accelerate degradation.

The p-values confirm these effects are statistically significant ($p \ll 0.05$). The *45°* angle leads to maximum erosion, exposure time exacerbates degradation, and the interaction shows that these factors together intensify mass loss.

Analysis 2: Effect of steel type and exposure time under erosion conditions

This analysis investigates the impact of steel type (AISI 304, AISI 316L, UB6) and exposure time on mass loss under simple erosion conditions. The results (Tab.7) show that both factors significantly affect mass loss, as confirmed by ANOVA p-values indicating statistical significance.

Table 7. Results of the analysis of variance (ANOVA) for studying the effects of steel type and exposure time on mass loss under erosion conditions.

Factor	F	Critical F value	p-value	Conclusion
Steel type	*120.96*	*3.31*	$\ll 0.05$	Type of steel has a substantial effect on erosion resistance
Exposure time	*65.9*	*2.68*	$\ll 0.05$	Exposure time has a statistically significant impact on mass loss. Degradation is amplified over time;
Interaction (angle × time)	*2.99*	*2.26*	< 0.05	The interaction between stainless steel type and exposure time is also significant, though less pronounced than the individual effects.

Steel type has a strong effect, with an F value of *120.96* exceeding the critical value of *3.31*. UB6 demonstrates the better resistance to erosion, followed by AISI 316L with moderate resistance, while AISI 304 is the most vulnerable, showing the greatest mass loss. Exposure time also has a significant effect, with an F value of *65.9* exceeding the critical value of *2.68*, demonstrating that degradation increases over time for all alloys.

The interaction between steel type and exposure time, with an F value of *2.99* exceeding the critical value of *2.26*, indicates that mass loss over time depends on the steel type. AISI 304 degrades rapidly over time, while UB6 remains stable, even during prolonged exposure.

The p-values confirm that these effects are statistically significant ($p \ll 0.05$). The choice of steel and exposure time strongly influence degradation, with UB6 consistently showing better resistance compared to AISI 316L and AISI 304.

Analysis 3: Effect of steel type and corrosive environment under erosion-corrosion conditions

This analysis evaluates the influence of stainless steel type (AISI 304, AISI 316L, UB6) and corrosive environment (neutral, saline, acidic) on mass loss under erosion-corrosion conditions. The results (Tab.8) confirm that both steel type and corrosive environment significantly affect mass loss, as shown by the ANOVA p-values.

Steel type significantly affects mass loss, with an F value of *5.67* exceeding the critical value of *3.55*. UB6 shows the better resistance, followed by AISI 316L with moderate resistance, while AISI 304 is the most susceptible. Similarly, the corrosive environment has a significant effect, with an F value of *14.76* exceeding

the critical value of *3.55*. Mass loss is highest in the acidic environment, moderate in the saline environment, and lowest in the neutral environment.

The interaction between steel type and corrosive environment, with an *F* value of *0.03* exceeding the critical value of *2.92*, indicates that sensitivity to erosion-corrosion depends on the environment. AISI 304 is particularly vulnerable in acidic conditions, where erosion and corrosion effects are most severe, while UB6 maintains its stability across all environments.

The *p*-values confirm these effects are statistically significant ($p \ll 0.05$). Steel type and environment both strongly influence mass loss, with UB6 demonstrating better resistance across all environments, while AISI 304 is particularly vulnerable in acidic conditions.

Table 8. Results of the analysis of variance (ANOVA) for studying the effects of steel type and corrosive environment on mass loss under erosion-corrosion conditions.

Factor	*F*	Critical *F* value	*p*-value	Conclusion
Steel type	*5.67*	*3.55*	$\ll 0.05$	The choice of steel significantly affects mass loss under erosion-corrosion conditions.
Test environment	*14.76*	*3.55*	$\ll 0.05$	The corrosive environment can amplify material degradation.
Interaction (steel × environment)	*0.03*	*2.92*	< 0.05	Steel sensitivity to erosion-corrosion depends on the environment;

Steel type significantly affects mass loss, with an *F* value of *5.67* exceeding the critical value of *3.55*. UB6 shows the better resistance, followed by AISI 316L with moderate resistance, while AISI 304 is the most susceptible. Similarly, the corrosive environment has a significant effect, with an *F* value of *14.76* exceeding the critical value of *3.55*. Mass loss is highest in the acidic environment, moderate in the saline environment, and lowest in the neutral environment.

The interaction between steel type and corrosive environment, with an *F* value of *0.03* exceeding the critical value of *2.92*, indicates that sensitivity to erosion-corrosion depends on the environment. AISI 304 is particularly vulnerable in acidic conditions, where erosion and corrosion effects are most severe, while UB6 maintains its stability across all environments.

The *p*-values confirm these effects are statistically significant ($p \ll 0.05$). Steel type and environment both strongly influence mass loss, with UB6 demonstrating better resistance across all environments, while AISI 304 is particularly vulnerable in acidic conditions.

4. Discussion

4.1. Analysis of cross-sectional microstructures after erosion testing at *45°*

The microstructural analysis of the cross-sectional images after erosion tests at a *45°* impact angle (Fig.14) in a neutral environment provides insight into the internal structure and affected zones of AISI 304, AISI 316L, and UB6 stainless steels. These observations highlight the varying degrees of surface damage caused by erosion-corrosion.

Microstructural analysis of AISI 304 surface degradation (Fig.14.a, Fig.14.b):

At 200x magnification, the cross-sectional view (Fig.14.a) reveals deep cavities and cracks extending into the material, indicating severe material loss and erosion-corrosion damage. The areas circled in red highlight significant surface degradation. At 20x magnification (Fig.14.b), the image shows widespread grain

boundary attacks and surface disruptions over a larger area, which further underline the instability of AISI 304's passive film [23]. These features confirm that AISI 304 experiences the most severe erosion-corrosion damage among the tested alloys.

The severe degradation observed in AISI 304 can be attributed to grain boundary instability and the formation of deep cracks under mechanical stress, which accelerate corrosion in acidic environments [23].

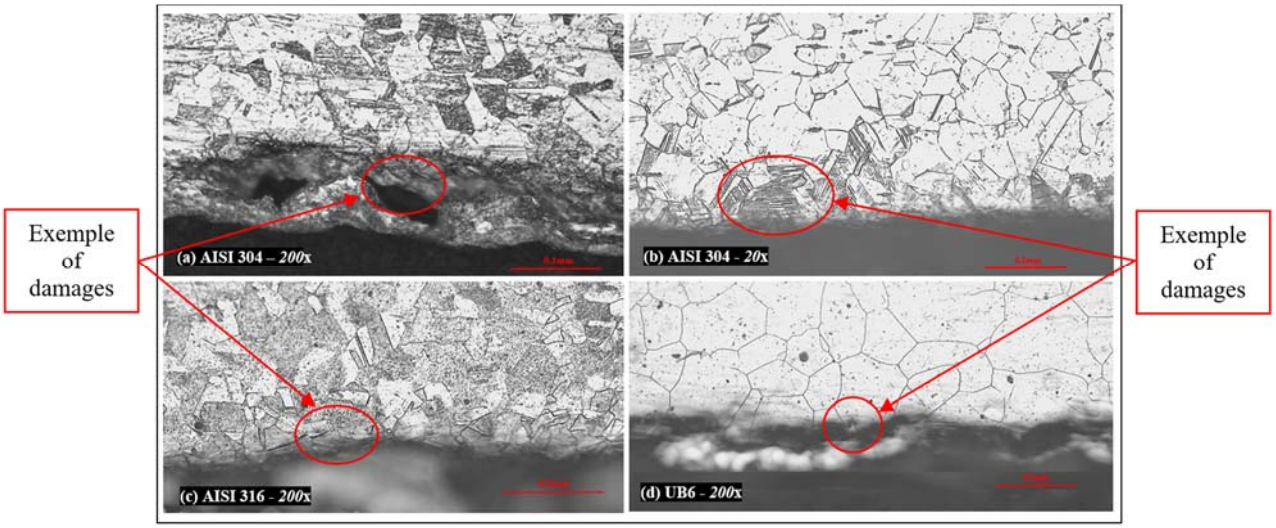

Fig.14. Cross-sectional images of the samples after the erosion test at a *45°* angle: (a) AISI 304, 200x; (b) AISI 304, 20x (c) AISI 316L, 200x; (d) UB6, 200x; magnification.

Microstructural analysis of AISI 316 surface degradation (Fig.14.c):

The cross-sectional view of AISI 316L at 200x magnification reveals moderate surface degradation characterized by shallow pits and surface roughening, as highlighted in red. AISI 316L shows less pronounced degradation compared to AISI 304, reflecting its improved resistance to erosion-corrosion [23].

Microstructural analysis of UB6 surface degradation (Fig.14.d):

At 200x magnification, the cross-sectional image of UB6 demonstrates minimal degradation, with small pits and a relatively smooth surface visible in the circled areas [19]. The absence of deep penetration and the low surface roughness are consistent with the previously measured roughness values for UB6 under neutral erosion conditions at a *45°* impact angle [19]. These observations confirm UB6's better resistance to erosion-corrosion, making it the most resistant alloy among those tested [19].

The minimal degradation of UB6, as evident in the cross-sectional image, can be linked to its stable microstructure, which resists crack propagation even under acidic conditions [19]. This suggests a limited synergy between erosion and corrosion in UB6, indicating that mechanical and electrochemical processes act more independently – a behavior consistent with Wood's low synergy category for erosion-resistant materials [27].

4.2. Synergy between erosion and corrosion

The results reveal a marked synergy between mechanical erosion and chemical corrosion, highlighting the combined influence of impact parameters, such as impact angle and environmental conditions, on the erosion-corrosion behavior of the tested stainless steels (AISI 304, AISI 316L, and UB6) [7, 8]. This synergy is evidenced by the significant increase in corrosion current density (J_{corr}) observed after abrasion [8].

In the absence of erosion, the naturally formed passive oxide layer serves as an effective protective barrier, maintaining low J_{corr} values. However, the introduction of erosion disrupts this equilibrium. Abrasive impacts weaken the passive film, exposing the underlying metal surface to corrosive agents [8]. This mechanical disruption leads to a substantial rise in J_{corr}, particularly in acidic and saline environments where the passive layer's self-repair capabilities are compromised [8].

As defined by Wood [27], the total synergistic effect (*S*) includes both erosion-enhanced corrosion (ΔC) and corrosion-enhanced erosion (ΔE). In our study, both mechanisms are evident: erosion removes the protective oxide layer, while corrosion promotes subsurface weakening, making the alloy more vulnerable to particle-induced removal – a feedback loop consistent with the high-synergy behavior described in his classification of erosion-corrosion interactions.

Impact of acidic environments on erosion-corrosion behavior

In acidic environments, H^+ ions accelerate the dissolution of the passive film, particularly in the micro-cracks and weakened zones created by erosion [8]. These damaged areas fail to repassivate effectively, leaving the bare metal exposed and vulnerable to rapid corrosion [8]. The presence of H^+ ions significantly amplifies the degradation process, making acidic conditions the most aggressive among the tested environments [8].
The pronounced synergy observed at a *45°* angle in acidic environments can be attributed to the combined action of high shear forces and acidic dissolution of the passive layer, which prevents passivation [8]. The synergy between erosion and corrosion is evident in the formation of intergranular cracks in AISI 304, where mechanical forces exacerbate the breakdown of protective oxide layers in acidic conditions [8].

These observations match well with the findings of Islam [28], who demonstrated that acidic media with H^+ ions destabilize protective films and exacerbate crack propagation, leading to intensified material loss when erosion and corrosion are coupled. This dual mechanism supports the dominance of erosion-enhanced corrosion, as acidic ions infiltrate freshly exposed surfaces, a key contributor to synergistic damage in Wood's framework [27].

Impact of saline environments on erosion-corrosion

In saline environments, Cl^- ions exploit the micro-cracks caused by erosion to initiate localized pitting corrosion [1]. Although the increase in J_{corr} is less pronounced compared to acidic conditions, the repeated mechanical disruption of the passive film prevents the formation of a stable protective barrier [1]. This results in continuous exposure of the metal surface to corrosive attacks [1].
In line with Islam [28], we observed that saline environments promote localized corrosion within mechanically induced surface cracks. These act as initiation sites, and the repeated failure of repassivation fosters the cyclic removal of weakened zones – a characteristic of moderate synergy intensity.

Erosion-corrosion resistance in neutral environments

In neutral environments, the effects of erosion are relatively minimal [21]. The passive oxide layer remains stable and is able to self-repair effectively due to the absence of aggressive ions like H^+ and Cl^- [21]. As a result, J_{corr} values remain low, and the material exhibits significantly higher resistance to erosion-corrosion [21].

According to Wood's classification of erosion-corrosion interactions [27], this scenario reflects a near-additive regime, where the total material loss (*T*) equals the sum of pure erosion (*E*), pure corrosion (*C*), and a minimal synergistic contribution (*S*).

$$T = E + C + S\,. \tag{4.1}$$

This behavior was evident for all tested materials in the neutral environment, with UB6 showing the lowest roughness and J_{corr} values – confirming a negligible interaction between erosion and corrosion under these conditions.

5. Conclusion

This study explored the erosion-corrosion behavior of stainless steels AISI 304, AISI 316L, and UB6 (AISI 904L) under various environmental conditions (neutral, saline, and acidic) and impact angles. The findings can be summarized as follows:

- AISI 304 showed the highest level of degradation, particularly at a *45°* impact angle in acidic environments, where the interaction between erosion and corrosion was most intense.
- AISI 316L exhibited moderate resistance, performing well in neutral and saline conditions but showing greater vulnerability in acidic environments.
- UB6 (AISI 904L) stood out for its exceptional resistance across all tested conditions, making it well suited for demanding applications involving combined erosion and corrosion.
- Microstructural observations confirmed these results, with severe damage seen in AISI 304, moderate wear in AISI 316L and minimal impact on UB6.
- Statistical analysis (ANOVA) emphasized the importance of impact angle and environment, identifying *45°* as the critical angle where erosion and corrosion effects combine most effectively.

Nomenclature

AISI – American Iron and Steel Institute
AISI 304 – austenitic stainless steel (*18%* Cr, *8%* Ni)
AISI 316L – austenitic stainless steel with molybdenum (*16%* Cr, *10%* Ni, *2%* Mo)
AISI 904L (UB6) – high-alloy austenitic stainless steel (*20%* Cr, *25%* Ni, *4%* Mo)
ANOVA – Analysis of Variance
C – pure corrosion loss
critical F-value – reference value for determining significance in ANOVA
Cl^- – chloride ion (primary corrosive agent in saline environments)
DIW – Deionized Water
DIZ – Direct Impact Zone (region of maximum mechanical erosion)
F-statistic – ratio of variance between groups to variance within groups (ANOVA)
H^+ – hydrogen ion (primary corrosive agent in acidic environments)
H_3PO_4/H_2SO_4 – phosphoric/sulfuric acid (components of acidic test medium)
HV – Vickers Hardness
impact angle – angle between abrasive jet and sample surface (*30°*, *45°*, *60°*)
J_{corr} – corrosion current density
NaCl – sodium chloride (simulated saline environment)
OCP – Open Circuit Potential
OA – Outer Area (peripheral region influenced by erosion-corrosion synergy)
p-value – probability value indicating statistical significance (threshold $- < 0.05$)
pH – measure of acidity/alkalinity (potential of hydrogen)
Ra – surface roughness – arithmetic mean deviation of surface profile (measured in μm)
S – the synergistic contribution
SEM – Scanning Electron Microscope
SCE – Saturated Calomel Electrode (reference electrode)
SiO_2 – silica – abrasive particles (*99.7%* purity, *0.23 mm* average size)
synergy factor – combined effect of erosion and corrosion exceeding individual contributions
T – total material loss due to erosion-corrosion

UB6 – stainless steel grade equivalent to AISI 904L

wt.% – weight percentage (chemical composition)

$\Delta m / m_o$ – mass loss ratio (dimensionless, reported as $\times 10^{-5}$)

$\Delta R / R_o$ – roughness ratio (dimensionless)

θ – impact angle (e.g., *30°*, *45°*, *60°*)

References

[1] López D., Congote J.P., Cano J.R., Toro A. and Tschiptschin A.P. (2005): *Effect of particle velocity and impact angle on the corrosion-erosion of AISI 304 and AISI 420 stainless steels*.– Wear, vol.259, pp.118-124.

[2] Ghasemi H.M., Karimi M., Pasha A. and Abedini M. (2011): *Erosion-corrosion behavior of 316-ss in seawater simulated environment at various impingement angles*.– International Journal of Mechanical and Materials Engineering, vol.6, pp.400-404.

[3] Rajahram S.S., Harvey T.J. and Wood R.J.K. (2010): *Full factorial investigation on the erosion-corrosion resistance of UNS S31603*.– Tribology International, vol.43, pp.2072-2083.

[4] Tian Y., Zhao H., Yang R., Liu X., Chen X., Qin J., McDonald A. and Li H. (2022): *In-situ SEM investigation on stress-induced microstructure evolution of austenitic stainless steels subjected to cavitation erosion*.– Materials & Design, vol.213, p.110314.

[5] Chellaganesh D., Adam Khan M., Ebenezer G. and Sivakumar S. (2021): *Erosion studies of SS316L using water jet machine for piping applications*.– Materials Today: Proceedings, vol.46, pp.7359-7363.

[6] El-Midany T.T., Abdel Samad A.A.F., Abdel Moneim A.M.G. and Saleh Y.S.A. (2016): *Effect of material type, impact angle and specimen shape on erosion process*.– Mansoura Engineering Journal (MEJ), vol.41, No.2, https://doi.org/10.21608/bfemu.2020.98792.

[7] Laguna-Camacho R., Marquina-Chávez A., Méndez-Méndez J.V. and Vite-Torres M. (2013): *Solid particle erosion of AISI 304, 316 and 420 stainless steels*.– Wear, vol.301, pp.254-262.

[8] Chung R.J., Jiang J., Pang C., Yu B., Eadie R. and Li D.Y. (2021): *Erosion-corrosion behaviour of steels used in slurry pipelines*.– Wear, vol.477, p.203771.

[9] Iversen B. and Leffler B. (2010): *Aqueous corrosion of stainless steels*.– Elsevier Reference Module in Chemistry, Molecular Sciences and Chemical Engineering, vol.3, pp.1802-1878.

[10] Yao J., Zhou F., Zhao Y., Yin H. and Li N. (2015): *Investigation of erosion of stainless steel by two-phase jet impingement*.– Applied Thermal Engineering, vol.88, pp.353-362.

[11] Wood R.J.K., Walker J.C., Harvey T.J., Wang S. and Rajahram S.S. (2013): *Influence of microstructure on the erosion and erosion-corrosion characteristics of 316 stainless steel*.– Wear, vol.306, pp.254-262.

[12] Ricardo G.A.N. and Sommerfeld M. (2020): *Experimental evaluation of surface roughness variation of ductile materials due to solid particle erosion*.– Advanced Powder Technology, vol.31, pp.3790-3816.

[13] Divakar M., Agarwal V.K. and Singh S.N. (2005): *Effect of the Material Surface Hardness on the Erosion of AISI316*.– Wear, vol.259, pp.110-117.

[14] Malik M., Toor I.H. and Ahmed W.H. (2014): *Evaluating the effect of hardness on erosion characteristics of aluminum and steels*.– Journal of Materials Engineering and Performance, vol.23, pp.2274-2282.

[15] Bassach P., Quintana G., Ferrer I. and Ciurana J. (2011): *Studying the relation between corrosion and surface roughness*.– AIP Conference Proceedings, vol.1431, pp.319-327.

[16] Toloei V., Stoilov V. and Northwood D. (2013): *The relationship between surface roughness and corrosion*.– ASME International Mechanical Engineering Congress and Exposition, pp.10, https://doi.org/10.1115/IMECE2013-65498

[17] Loto R.T. (2017): *Study of the corrosion resistance of type 304L and 316 austenitic stainless steels in acid chloride solution*.– Oriental Journal of Chemistry, vol.33, pp.1090-1096.

[18] Zhang J., Ju P., Wang C. and Yuchao D. (2019): *Corrosion behaviour of 316L stainless steel in hot dilute sulphuric acid solution with sulphate and NaCl*.– Prot. Met. Phys. Chem. Surf., vol.55, pp.148-156.

[19] Karafyllias G., Galloway A. and Humphries E. (2021): *Erosion-corrosion assessment in strong acidic conditions for a white cast iron and UNS S31600 stainless steel*.– Wear, vol.484-485, p.203665.

[20] Tan L., Wang Z. and Ma Y. (2021): *Tribocorrosion behavior and degradation mechanism of 316L stainless steel in typical corrosive media*.– Acta Metallurgica Sinica, vol.34, pp.813-824.

[21] Gudić S., Kvrgić D., Vrsalović L. and Gojić M. (2018): *Comparison of the corrosion behavior of AISI 304, AISI 316L, and duplex steel in chloride solution*.– Zastita Materijala, vol.59, pp.307-315.

[22] Lindgren M., Siljander S., Suihkonen R., Pohjanne P. and Vuorinen J. (2016): *Erosion-corrosion resistance of various stainless steel grades in high-temperature sulfuric acid solution*.– Wear, vol.364-365, pp.11-21.
[23] Li H., Yang X., Yin X., Wang X., Tang J. and Gong J. (2021): *Effect of chloride impurity on corrosion kinetics of stainless steels in molten solar salt for CSP application*.– Oxidation of Metals, vol.95, pp.311-332.
[24] Neshati J., Shirazani T.S.T. (2009): *Electrochemical behaviour of stainless steel 304 alloy in erosion-corrosion conditions and synergism effect*.– Tribology – Materials, Surfaces & Interfaces, vol.3, No.3, pp.103-109.
[25] Andrews N., Giourntas L., Galloway A.M. and Pearson A. (2014): *Effect of impact angle on the slurry erosion-corrosion of Stellite 6 and SS316*.– Wear, vol.320, pp.143-151, DOI:10.1016/j.wear.2014.08.006.
[26] Zhao Y.-L., Tang C.-Y., Yao J., Zeng Z.-H. and Dong S.-G. (2020): *Investigation of erosion behavior of 304 stainless steel under solid-liquid jet flow impinging at 30°*.– Petroleum Science, vol.17, pp.1135-1150.
[27] Wood R.J. (1992): *Erosion-corrosion synergism for multi-phase flow line materials*.– La Houille Blanche, vol.7, No.8, pp.3-8.
[28] Islam A., Farhat Z.N., Ahmed E.M. and Alfantazi A.M. (2013): *Erosion enhanced corrosion and corrosion enhanced erosion of API X-70 pipeline steel*.– Wear, pp.1-10.
[29] Brownlie F., Hodgkiess T., Pearson A. and Galloway A.M. (2021): *Erosion corrosion mechanisms of engineering steels in different NaCl concentrations*.– Journal of Bio- and Tribo-Corrosion, vol.7, No.80, DOI:10.1007/s40735-021-00519-2.

Received: February 18, 2025
Revised: August 13, 2025